

Formation of Heavy Residues with $A < 90$ in
 the Asymmetric Reaction of 20 AM eV
 $^{124}\text{Sn} + ^{27}\text{Al}$ as a Sensitive Probe of the
 Multifragmentation Process

M. Veselsky^{a,b}, G.A. Souliotis^b, G.C. Chubarian^b, L. Trache^b,
 A. Keksis^b, E.M. Martin^b, A. Ruangma^b, E.W. Winchester^b, and
 S.J. Yennello^b.

^aInstitute of Physics, Slovak Academy of Sciences, Dúbravská 9, 84228 Bratislava,
 Slovakia

^bCyclotron Institute, Texas A & M University, College Station, TX 77843, USA

Abstract

The cross sections and velocity distributions of heavy residues from the reaction of 20 AM eV $^{124}\text{Sn} + ^{27}\text{Al}$ have been measured at forward angles using the MARS recoil separator at Texas A & M in a wide mass range. A consistent overall description of the measured cross sections and velocity distributions was achieved using a model calculation employing the concept of deep-inelastic transfer for the primary stage of peripheral collisions, pre-equilibrium emission and incomplete fusion for the primary stage of more violent central collisions and the statistical model of multifragmentation (SMF) for the deexcitation stage. An analogous calculation employing the evaporation code GEMINI featuring the sequential binary decay could not reproduce the observed yields of the residues from violent collisions ($A < 90$) due to different kinematic properties. The simultaneous character of the multifragmentation process leading to the observed residues from violent collisions is thus demonstrated.

Key words: Nuclear reactions, intermediate energy, peripheral collisions, violent collisions, sequential binary decay, simultaneous multifragmentation.

PACS: 25.70.-z, 25.70.Hj, 25.70.Lm

¹ E-mail address: fyziarv@savba.sk (M. Veselsky).

1 Introduction

The yields of the heavy residues, the large remnants of the heavy member of an asymmetric reacting pair of nuclei, are known to comprise a large fraction of the reaction cross section for intermediate energy nuclear collisions. The studies carried out in inverse kinematics at projectile energies of several tens of AM eV by Bazin et al. [1], Faure-Ramstein et al. [2], Pfa et al. [3], Hanold et al. [4] and Souliotis et al. [5,6] have shown the utility of the fragment separator approach in studying the heavy reaction products from $Kr + X$, $X + X$ and $^{197}Au + X$ mass asymmetric collisions at intermediate energies. Compared to asymmetric reactions in normal kinematics [7,8], where the low energies of residues (0.015 AM eV) cause the loss of substantial portions (50%) of the product distributions, due to experimental thresholds [7], the studies in inverse kinematics using a high resolution spectrometer/detector system allow the observation of a wide range of nuclei including the projectile-like fragments (PLFs) and the heavy remnants of the hot nuclei originating from violent collisions. From such inclusive measurement, one can gain important information about the reaction mechanism, complementary to that obtained in exclusive studies, where only the light reaction partners are observed with high isotopic resolution.

For asymmetric reactions of a heavy beam with a light target nucleus (typically ^{197}Au) the momentum transfer data obtained (see e.g. [2,4,5]) demonstrate the presence of reaction mechanisms ranging from quasi-elastic peripheral collisions to processes analogous to the complete-fusion and incomplete-fusion observed at low energies. However, since asymmetric reactions at several tens of AM eV are complex processes, the description of the data by the simple low energy concepts such as massive transfer hypothesis or the high-energy geometric abrasion model have shown to be, despite qualitative agreement, far from quantitative.

With increasing target mass, the reactions become more symmetric and the observed yields of heavy residues are dominated by peripheral processes such as deep-inelastic transfer as, for instance, shown in detail in our recent work [9] in the reaction of 25 AM eV $^{86}Kr + ^{64}Ni$. As it follows from the model analysis (for details see the original work), the projectile-like fragments observed in this reaction are heated by intense exchange of nucleons with the target. The excitation energy is sufficient for emission of complex fragments. Previous studies [1,10,11,12,13,14,15,16,17,18] of the collisions of heavy nuclei at intermediate energies have also shown that such collisions are predominantly binary. Evidence has been presented [18] for a sequential decay of one of the initial binary fragments leading to a three (or more) body final state. In some of the binary encounters the projectile-like fragments have been found [14,17] to have very high temperatures ($T \approx 7$ MeV).

The focus of the present work is the formation of heavy residues in the reaction of 20 AM eV ^{124}Sn on ^{27}Al . The main motivation was the observation of heavy remnants of hot nuclei created in violent collisions at low impact parameters where one hot source is created. In particular, it is of importance to establish in detail to what extent the observed properties of such heavy residues are influenced by the dynamics of the entrance channel (pre-equilibrium emission, incomplete fusion) and/or by the process of de-excitation (emission of complex fragments, multifragmentation). In the reaction $^{124}\text{Sn} + ^{27}\text{Al}$ one can assume that the residues with masses much lower than that of the beam originate from violent collisions. Such an assumption is supported by the work presented in [19], where it was shown that for the damped peripheral collisions $^{28}\text{Si} + ^{112,124}\text{Sn}$ at energies 30 { 50 AM eV the heavy target-like fragment remains rather cold, while the light projectile-like fragment is hot enough to undergo multifragmentation. This is caused by approximately equal sharing of the excitation energy imparted to the reaction partners due to nucleon exchange. In order to heat the heavy fragment to higher excitation energies, part of the lighter partner should fuse with the heavier one, thus converting the kinetic energy of the relative motion into heat. The recoil spectrometer MARS at the Cyclotron Institute of Texas A & M University offers the possibility to carry out this study with an appropriate angular and momentum acceptance, under high-resolution conditions and in the appropriate region of nuclei.

2 Experimental Method and Data Analysis

The present study was performed at the Cyclotron Institute of Texas A & M University. A 20 AM eV $^{124}\text{Sn}^{27+}$ beam from the K 500 superconducting cyclotron, with a typical current of 0.5 pA, interacted with a ^{27}Al target of thickness 2.0 mg/cm². The reaction products were analyzed with the MARS recoil separator [20]. The primary beam struck the target at 0° relative to the optical axis of the spectrometer. The direct beam was collected in a small square Faraday cup approx. 30 cm after the target, blocking the angular range 0.0{1.0°. The fragments were accepted in the remaining angular opening of MARS: 1.0{2.7° (the angular acceptance of MARS is 9 m sr [20]). This angular range encompasses the grazing angle of 2.1° [21] for the present reaction. MARS optics [20] provides one intermediate dispersive image and a final achromatic image (focal plane) and offers a momentum acceptance of 4%.

At the focal plane, the fragments were collected in a large area (5 { 5 cm) three-element (E_1, E_2, E) Si detector telescope. The E_1 detector was a position-sensitive Si strip detector of 63 μm thickness, whereas the E_2 and the E detector were single-element Si detectors of 150 and 950 μm, respectively. The position information from the E_1 strips provided a continuous monitoring of the focusing and collection of the fragments at the various settings of the

separator. Time of flight was measured between two parallel plate avalanche counters (PPACs) [22] positioned at the dispersive image and at the focal plane, respectively, and separated by a distance of 13.2 m. The PPAC at the dispersive image was also X {Y position sensitive and used to record the position of the reaction products. The horizontal position, along with NMR measurements of the field of the MARS first dipole, was used to determine the magnetic rigidity B of the particles. Thus, the reaction products were characterized by an event-by-event measurement of the energy loss, residual energy, time of flight, and magnetic rigidity. The response of the spectrometer and detector system to ions of known atomic number Z , mass number A , ionic charge q and velocity was calibrated using low intensity primary beams of ^{124}Sn at 20 AMeV and ^{40}Ar , ^{44}Ca and ^{86}Kr at 25 AMeV. To cover the N/Z and velocity range of the fragments, a series of measurements was performed at overlapping magnetic rigidity settings in the range 1.3{1.6 Tesla-meters.

The determination of the atomic number Z was based on the energy loss of the particles in the first E detector [23] and their velocity, with a resulting resolution (FWHM) of 1.0 Z units for near-projectile fragments and 0.6 Z units for $A < 90$. The ionic charge q of the particles after the Al stripper, was obtained from the total energy $E_{\text{tot}} = E_1 + E_2 + E$, the velocity and the magnetic rigidity according to the expression:

$$q = \frac{3.107}{931.5B} \frac{E_{\text{tot}}}{(1 - 1)} \quad (1)$$

where E_{tot} is in MeV, B in Tm, $c = =c$ and $1 = (1 - v^2)^{\frac{1}{2}}$. The measurement of the ionic charge q had a resolution of 0.8 Q units (FWHM) for near-projectile fragments and 0.5 Q units for $A < 90$. Since the ionic charge must be an integer, we assigned integer values of q for each event by putting appropriate windows on each peak of the q spectrum at each magnetic rigidity setting of the spectrometer. Using the magnetic rigidity and velocity measurement, the mass-to-charge A/q ratio of each ion was obtained from the expression:

$$A = q = \frac{B}{3.107} \quad (2)$$

Combining the q determination with the A/q measurement, the mass A was obtained as:

$$A = q_{\text{int}} \quad A = q \quad (3)$$

(q_{int} is the integer ionic charge determined as above) with an overall resolution (FWHM) of 1.0 A units for near-projectile fragments and about 0.6 A units for $A < 90$. We refer to our previous work in ref. [9], carried out using

the same experimental setup within the same run, for more details. The reconstruction of the Z , q and A and the gating procedure were applied to the calibration beam data to ensure the reproduction of the expected Z , q and A values and the elimination of spurious yield contributions from neighboring Z and q values. For the heavier products with masses $A > 90$ the experimental resolutions did not allow the mass to be resolved unambiguously. However, the gross features for such products can be still obtained. Close to the beam, part of the yield could not be detected due to background from the elastically scattered beam.

Combination and appropriate normalization of the data at the various magnetic rigidity settings of the spectrometer provided fragment distributions with respect to Z , A , q and velocity. Correction of missing yields caused by charge changing at the PPAC (positioned at the dispersive image) was performed based on the equilibrium charge state prescriptions of Leon et. al. [24]. The overall data reduction procedure was similar to that followed in earlier work on ^{197}Au fragmentation [6] and ^{238}U projectileission [25] at 20 AM eV. The isotope distributions were subsequently summed over all values of q . It should be pointed out that the resulting distributions in Z , A and velocity are the fragment yield distributions in the reaction angle interval $1.0\{2.7^\circ$ in the magnetic rigidity range $1.3\{1.6$ T m.

3 Results and Discussion

The gross features of the measured data from the reaction of 20 AM eV ^{124}Sn + ^{27}Al are displayed in Figs. 1,2. In Fig. 1 isotopic yields (contour plot) are presented as a function of mass and atomic number. The masses of observed products cover the range from the projectile-like fragments to the border of the intermediate mass fragment domain at $Z=20$. The yields of projectile-like nuclei peak around the nuclide ^{116}Te . The position of this peak is caused by missing yield from the region close to the beam where the reaction products cannot be resolved using the existing detector set-up due to significant background from elastic processes. At masses below $A=90$ the distribution becomes rather flat and follows approximately the corridor of stable isotopes (thick dashed line). These are the reaction products which are expected to originate from the hot excited systems. Fig. 2 presents the momentum distributions of residues with selected atomic numbers. In the region close to beam the momentum distributions appear to be convolutions of multiple contributions from different reaction channels ranging from quasielastic products close to the beam velocity to various incomplete fusion channels where the velocity decreases with the amount of mass transferred from the target. With decreasing mass of the reaction product the momentum distributions develop toward a single contribution of a Gaussian shape with a low momentum tail. The

centroids of these distributions shift with decreasing mass toward higher momentum. Such a trend is caused by the kinematic selection of the spectrometer imposed by the B_{π} selection in the region $1.3\{1.6$ T m.

The experimental heavy residue data presented in Figs. 1,2 contains useful information on the production mechanism. The properties of the final products are the result of a complex process including an early stage dominated by the dynamics of the entrance channel which is governed by the impact parameter and a de-excitation stage where the final partitions of the reaction products are generated. In such a case, a viable method of reaction mechanism analysis appears to be the use of various model frameworks for both the initial stage of the collision and the de-excitation. The model which eventually proves superior to others can be considered as reflecting the actual physical process in most detail.

As a first choice for the description of the initial stage we use the model framework described in [26]. The basic features of the reaction mechanism model for violent collision are the pre-equilibrium emission and the incomplete fusion (ICF). The pre-equilibrium emission is treated using a variant of the exciton model employing phenomenological parameterization of emission probability as a function of exciton number and angular momentum. The incomplete fusion model is based on the concept of geometrical fragmentation refined for the Fermi energy domain where incomplete fusion occurs by fusion of the participant zone with one of the spectators. It is applied to the reconstructed projectile-like and target-like prefragments formed in the pre-equilibrium stage. For the dissipative peripheral collisions the model of deep inelastic transfer (DIT) is used as implemented by Tassan-Got and Stefan [27]. Again the DIT stage is preceded by the pre-equilibrium stage. Such a hybrid model framework proved rather successful [26] in the description of a wide range of data obtained in experiments ranging from inclusive measurements to highly exclusive ones in 4 geometry. Throughout the paper, this calculation will be named for simplicity as DIT + ICF. Nevertheless, one has to keep in mind that pre-equilibrium emission is included in this model.

In order to describe the de-excitation stage of hot nuclei, there exist several concepts implemented in various codes. The statistical deexcitation code GEMINI [28] uses Monte Carlo techniques and the Hauser-Feshbach formalism to calculate the probabilities for fragment emission with $Z \geq 2$. Heavier fragment emission probabilities are calculated using the transition state formalism of Moretto [29]. Within such a model, the final partition of products is generated by a succession of fragment emissions (binary decays). An alternative to this scenario is the model of statistical multifragmentation, where the fragment partition is generated at once in the so-called freeze-out configuration. In this work, we use the code SMILE [30] as a representative implementation of the concept of prompt multifragmentation.

The results of the D IT + ICF /GEM IN I calculation, compared to experimental observables are given in Fig. 3. In the GEM IN I calculations, we used Lestone's temperature dependent level density parameter [31], a fading of shell corrections with excitation energy and we enabled IMF emission. This parameter set proved successful in our recent work [9] on the reaction $^{86}\text{Kr} + ^{64}\text{Ni}$ at 25 AM eV.

In Fig. 3a the mass yield curve is presented. The measured data, normalized for beam current and target thickness are given in mb and presented as solid circles. The result of the D IT + ICF /GEM IN I calculation, filtered by the spectrometer angular and momentum acceptance is given by the full line, whereas the dashed line gives the total (unfiltered) yield. A comparison of the measured yields to the calculated filtered yields shows reasonable agreement for the heavier projectile-like fragments ($A > 90$). The missing experimental cross section at the masses close to the beam is caused by the limitations of the experimental set-up as explained in the discussion of Fig. 1. The yields of residues with $A < 90$ are increasingly underestimated by the calculation despite the fact that the unfiltered calculated yields are rather flat in this region, which appears to reflect the trend of the experimental data. The missing filtered yield below $A = 90$ in the calculation is caused by the fact that kinematic properties of the residues do not match the spectrometer acceptance what leads to their loss in the filtering procedure.

In Fig. 3b, the calculated and measured yield distributions as a function of Z (relative to the line of stability, Z_c) and A are presented. The line of stability is calculated as: $Z_c = A / (1.98 + 0.0155A^{2/3})$ [32]. The calculated values from D IT + ICF /GEM IN I are shown as a thick dashed line (without acceptance cut) and as a thick full line (with spectrometer acceptance cut). The measured yield distribution is represented by a contour plot. The D IT + ICF /GEM IN I calculation describes reasonably well the centroids of the experimental data.

Finally, in Fig. 3c, the velocity vs. mass distributions are given. The data are again shown as contours. The thick dashed line is from the D IT + ICF /GEM IN I calculation without acceptance cut and the full line is with acceptance cut. In this case the filtered calculated data appear to follow the experimental trend at masses above $A = 90$, while they exhibit rather steep increase of the mean velocity with decreasing masses below $A = 90$. This observation is consistent with the comparison of trends in Fig. 3a.

A complementary calculation was carried out, where the SM M code was used for the de-excitation of the hot nuclei produced by the D IT + ICF simulation. In the SM M calculation, a freeze-out configuration with hot primary fragments was assumed. Hot fragments are de-excited by secondary emission. The results are presented in Fig. 4 in a fashion analogous to Fig. 3. As one can see in all panels of Fig. 4, the D IT + ICF /SM M calculation provides very consistent de-

scription of experimental observables (the discrepancies in the region close to the beam are analogous to previous cases). Using the ratio of iterated to uniterated calculated yield for each mass, correction factors (whose magnitude are inferred from Fig. 4a) for the acceptance of the spectrometer can be obtained as a function of mass. When applied to the measured yield data, an estimate of the total yield, given by the open circles in Fig. 4a, could be obtained.

Thus, implementation of the prompt multifragmentation scenario appears to lead to residues with proper kinematics. Compared to light particles or intermediate mass fragments (IMFs) used for imaging of the emitting source via particle-particle correlations, the experimentally detected heavy remnants of multifragmentation possess direct information on the final state of the multifragmentation process. The process of secondary emission, as can be concluded from the simulations, does not influence dramatically the kinematic properties of the heavy residues with masses $A = 40\{90$, since emission of nucleons is a dominating channel of secondary de-excitation.

Detailed insight into different kinematic properties of residues simulated using GEM IN I and SM M codes can be obtained from Figs. 5,6,7. In Fig. 5 the calculated angular distributions as a function of residue mass for GEM IN I (a) and SM M (b) are presented. Two horizontal lines mark the angular acceptance of the MARS separator. It is remarkable to notice that, in fact, the gross features of both distributions are very similar and the experimental effect appears to be caused by the distant tail of the distribution, which extends much further toward zero angle in the scenario where the hot nucleus disintegrates simultaneously. In the case when the hot nucleus disintegrates by sequential binary decay, the recoil from emitted fragments causes the shift of the residue angle away from zero. In Figs. 6,7 are given the calculated velocity distributions as a functions of masses obtained using GEM IN I and SM M codes, respectively. In both cases, uniterated yields are presented in panel (a) while the iterated yields are given in panel (b). It is again quite remarkable how different velocity distributions can be obtained from the same initial sample of hot nuclei using the two de-excitation codes. Naively, one can identify the wedge-like structures in uniterated distributions with the "hot" source. Then, the apparent momentum transfer would differ by about 50 % since in the GEM IN I calculation it is centered at velocity $= 0.18$, while in the SM M calculation the center lies at velocity $= 0.17$.

In Fig. 8 are given the normalized uniterated residue mass distributions at various impact parameters for both calculations. For DIT + ICF /SM M one can notice a rather strong dependence of production rate for residues with $A < 90$ on impact parameter. For DIT + ICF /GEM IN I calculation, the dependence is rather weak. Significant contribution of $A < 90$ residues is produced already at $b = 8$ fm and toward lower impact parameters the shape of the distribution changes only moderately. As one can see in Fig. 9a, the average excitation

energy of the hot source obtained using DIT + ICF simulation changes with impact parameter rather strongly. At $b = 8$ fm, the average excitation energy amounts only to 80 MeV, which translates into relative excitation below 1 AMeV. At such excitation energy, the emission of IMFs is rather improbable and the simulated residues with $A < 90$ can be expected to be emission fragments in the traditional sense. In GEMINI calculation such emission fragments are produced with a probability of about two orders of magnitude larger than in SM calculation. This rather large difference reflects different treatment of emission in both codes. The code GEMINI uses the asymmetry-dependent emission barriers normalized to angular momentum dependent emission barriers of Sierk [33] while the SM code, where emission and multifragmentation are treated separately, uses the emission barriers of Barashenkov [34] without explicit angular momentum dependence. For example, the nucleus ^{124}Sn at angular momentum $J=0$ is supposed to have the emission barrier of 41.5 MeV in GEMINI and 44.8 MeV in SM. At $J=25$, which is a typical value of angular momentum at $b = 8$ fm (see Fig. 9b), the emission barrier of Sierk drops further to 36.9 MeV. Assuming a level density parameter $a = A/10$, the difference of level density indeed amounts to slightly less than two orders of magnitude, consistent with Fig. 8. Thus the production rates of residues with $A < 90$ at $b = 8$ fm are consistent with the production rates of emission fragments. An analogous conclusion applies to impact parameter $b = 6$ fm. At central impact parameters $b = 4$ fm and $b = 2$ fm, where the average relative excitation energy approaches and exceeds 2 AMeV, the simulated production rate of residues with $A < 90$ increases dramatically in the SM calculation and exceeds the production rate of GEMINI calculation. This is apparently caused by the fact that, in SM, the multifragmentation threshold is exceeded by increasing part of the excitation energy distributions (for simulated excitation energy distribution as a function of impact parameter see Fig. 10), while in GEMINI the onset of multifragment channels, within the sequential binary decay scenario, is much smoother. Furthermore, the residues with $A < 90$ from multifragment events generated by SM do have kinematic properties which comply better to the separator angular and momentum acceptance.

For further comparison, the simulations using only the model of deep inelastic transfer combined with both GEMINI and SM, analogous to DIT/GEMINI simulation used in our recent work [9], have been carried out. In the case of symmetric reaction $^{86}\text{Kr} + ^{64}\text{Ni}$ at 25 AMeV in [9], the DIT/GEMINI simulations proved to be rather successful. Similar success was achieved in the reaction of 20 AMeV $^{124}\text{Sn} + ^{124}\text{Sn}$ [35], especially for the residues with $A < 90$ on which this work focuses. It was verified using both DIT/GEMINI and DIT/SM that, in the reaction $^{124}\text{Sn} + ^{27}\text{Al}$ at 20 AMeV, the yields of residues with $A < 90$ can not be reproduced by simulations taking into account peripheral processes only, independent of which de-excitation code was used. For instance, in DIT/GEMINI simulations, the total uniterated yields are roughly analogous to the simulation presented in Fig. 3 and the iterated

yields again do not reproduce the observed yields of residues with $A < 90$. In this case, the itered distribution exhibits similar decrease in the $A < 90$ region but extends further than in D IT + ICF / GEM IN I case, due to higher excitation energy and different angular and momentum distribution of the generated hot nuclei. The difference can be attributed mostly to the absence of cooling via pre-equilibrium emission since the products of violent collisions are not included in the D IT / GEM IN I simulation and do not pass the iter procedure in the latter case. On the other hand, the D IT / SM M simulation, when compared to D IT + ICF / SM M simulation shown in Fig. 4, significantly underpredicts the yields of the residues with $A < 90$ (both un itered and itered), due to the fact that for the peripheral collisions the excitation energy of projectile-like fragments exceeds the value of 2 AM eV, where the multifragmentation threshold can be anticipated, only very rarely, and due to the orbiting, such sources move typically at angles away from zero.

From the comparison of the measured yields with the results of simulations one can conclude that the heavy residues with $A < 90$ observed in the experiment are produced in violent collisions at low impact parameters where one hot source is created by incomplete fusion which further de-excites via simultaneous multifragmentation. The production of such residues can not be explained either by peripheral collisions or by fission and sequential decay of the hot source. The D IT + ICF / SM M simulation proved to be a rather realistic model framework for the description of asymmetric nucleus-nucleus collisions at projectile energy around the Fermi energy, allowing to describe the experimental data quantitatively with a considerable level of consistency.

4 Summary and conclusions

In the present work, the cross sections and velocity distributions of heavy residues from the reaction of 20 AM eV ^{124}Sn on ^{27}Al have been measured at forward angles using the MARS recoil separator at Texas A & M. A consistent overall description of the measured cross sections and velocity distributions was achieved using a model calculation employing the concept of deep-inelastic transfer for the primary stage of the peripheral collisions, pre-equilibrium emission and incomplete fusion for the primary stage of the more violent central collisions and the statistical model of multifragmentation (SM M) for the de-excitation stage. An analogous calculation employing the de-excitation code GEM IN I featuring the sequential binary decay could not reproduce the observed yields of the residues from violent collisions ($A < 90$) since the angular distributions of the generated residues do not extend far enough toward zero angle. An assumption of simultaneous character of the multifragmentation process leading to the observed residues from violent collisions is found to be necessary for explanation of these data. Simulation of de-excitation via sequen-

tial emission results in a stronger recoil in the transverse direction, due to the fact that the probability density at low angles drops considerably with each emission. In simultaneous multifragmentation, which can be considered as a single emission act, the angular distribution of heavy residues is determined by the kinematics of the freeze-out configuration which is less restrictive at low angles. As demonstrated in the present work, a high resolution measurement using a kinematic separator is a sensitive method allowing to distinguish between these de-excitation scenarios.

5 Acknowledgment

We gratefully acknowledge the support of the operations staff of the Cyclotron Institute during the measurements. We express our gratitude to L. Tassan-Got for the opportunity to use his DIT code, to R. Charity for the use of the GEM-IN1 code and to A. S. Botvina for the use of the SM1 code. Financial support for this work was given, in part, by the U.S. Department of Energy under Grant No. DE-FG03-93ER40773, by the Robert A. Welch Foundation under Grant No. A-1266 and by Slovak Scientific Grant Agency under Grant No. VEGA-2/1132/21. M.V. would like to express his gratitude to the Cyclotron Institute of Texas A & M University for hospitality during his stay.

References

- [1] D. Bazin et al., *Nucl. Phys. A* 515 (1990) 349.
- [2] B. Faure-Ramstein et al., *Nucl. Phys. A* 586 (1995) 533.
- [3] R. Pfa et al., *Phys. Rev. C* 53 (1996) 1753.
- [4] K. A. Hanold et al., *Phys. Rev. C* 52 (1995) 1462.
- [5] G. A. Soulis et al., *Phys. Rev. C* 57 (1998) 3129.
- [6] G. A. Soulis et al., *Nucl. Phys. A* 705 (2002) 279.
- [7] K. A. Lekkert et al., *Nucl. Phys. A* 149 (1989) 591.
- [8] W. Loveland et al., *Phys. Rev. C* 41 (1990) 973.
- [9] G. A. Soulis et al., *Phys. Lett. B* 543 (2002) 163.
- [10] O. Graniier et al., *Nucl. Phys. A* 481 (1988) 109.
- [11] H. Barz et al., *Phys. Rev. C* 46 (1992) R42.
- [12] A. Yokoyama et al., *Phys. Rev. C* 46 (1992) 647.

[13] A. A. Marchetti et al., *Phys. Rev. C* 48 (1993) 266.

[14] M. Abou Rass et al., LPCC 93-14, September, 1993; J. F. Le Colley et al., *Phys. Lett. B* 325 (1994) 317.

[15] E. J. Garcia-Solis et al., *Phys. Rev. C* 52 (1995) 3114.

[16] S. P. Baldwin et al., *Phys. Rev. Lett.* 74 (1995) 1299.

[17] M. Morjean et al., *Nucl. Phys. A* 591 (1995) 371.

[18] D. G. d'Enterria et al., *Phys. Rev. C* 52 (1995) 3179.

[19] M. Veselsky et al., *Phys. Rev. C* 62 (2000) 64613.

[20] R. E. Tribble, R. H. Burch and C. A. Gagliardi, *Nucl. Instr. and Meth. A* 285 (1989) 441; R. E. Tribble, C. A. Gagliardi and W. Liu, *Nucl. Instr. and Meth. B* 56/57 (1991) 956.

[21] W. W. Wilke et al., *At. Data and Nucl. Data Tables* 25 (1980) 389.

[22] G. Chubarian, private communication.

[23] F. Hubert, R. Bimbot and H. Gauvin, *At. Data and Nucl. Data Tables* 46 (1990) 1. and *Nucl. Instrum. Methods B* 36 (1989) 357.

[24] A. Leon et al., *At. Data and Nucl. Data Tables* 69 (1998) 217.

[25] G. A. Soulis et al., *Phys. Rev. C* 55 (1997) R2146.

[26] M. Veselsky, *Nucl. Phys. A* 705 (2002) 193.

[27] L. Tassan-Got, and C. Stefan, *Nucl. Phys. A* 524 (1991) 121.

[28] R. Charity et al., *Nucl. Phys. A* 483 (1988) 391. The version of GEMINI included modifications made up to July, 1998.

[29] L. G. Moretto, *Nucl. Phys. A* 247 (1975) 211.

[30] J. P. Bondorf et al., *Phys. Rep.* 257 (1995) 133.

[31] J. Lestone, *Phys. Rev. C* 52 (1995) 118.

[32] P. Marmier and E. Sheldon, *Physics of Nuclei and Particles*, Volume I (Academic, New York, 1970) p. 15.

[33] A. J. Sierk, *Phys. Rev. C* 33 (1986) 2039.

[34] V. S. Barashenkov, A. S. Iljinov, V. D. Toneev, F. G. Gereghi, *Nucl. Phys. A* 206 (1973) 131.

[35] G. A. Soulis et al., in Proc. of EMIS-14 conference, Victoria, BC, May 2002, to appear in *NIM B*.

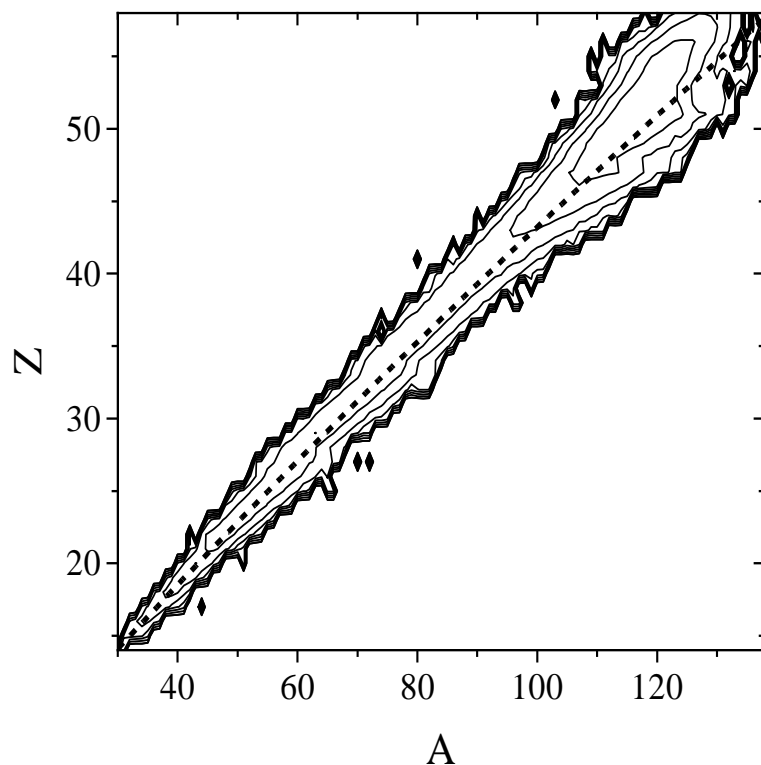


Fig. 1. Isotopic yields (contour plot) for the reaction 20 AM eV $^{124}\text{Sn} + ^{27}\text{Al}$ as a function of mass and atomic number. The corridor of stable isotopes is given by a thick dashed line.

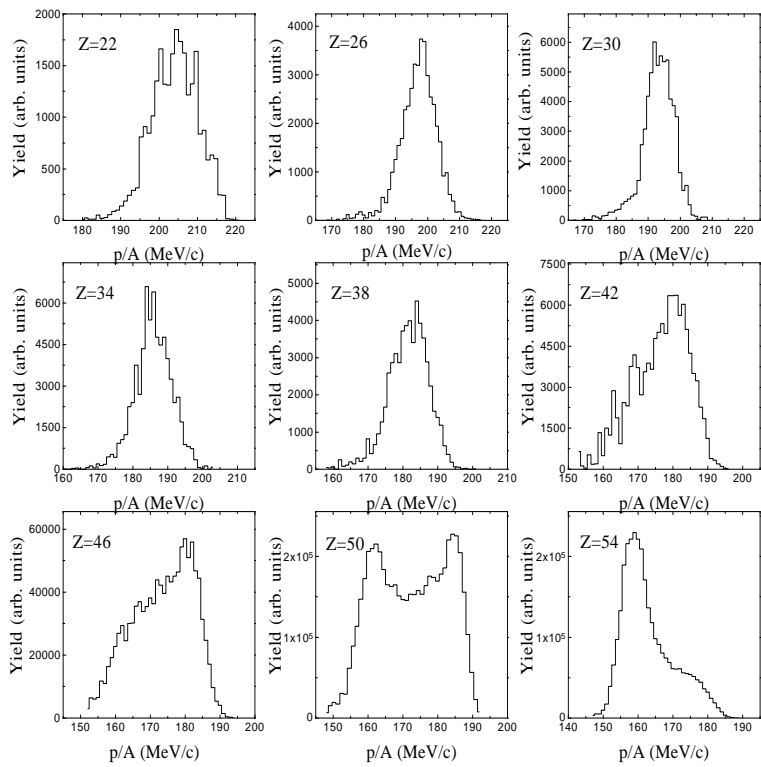


Fig. 2. Momentum distributions of residues with selected atomic numbers measured in the reaction 20 AMeV $^{124}\text{Sn} + ^{27}\text{Al}$.

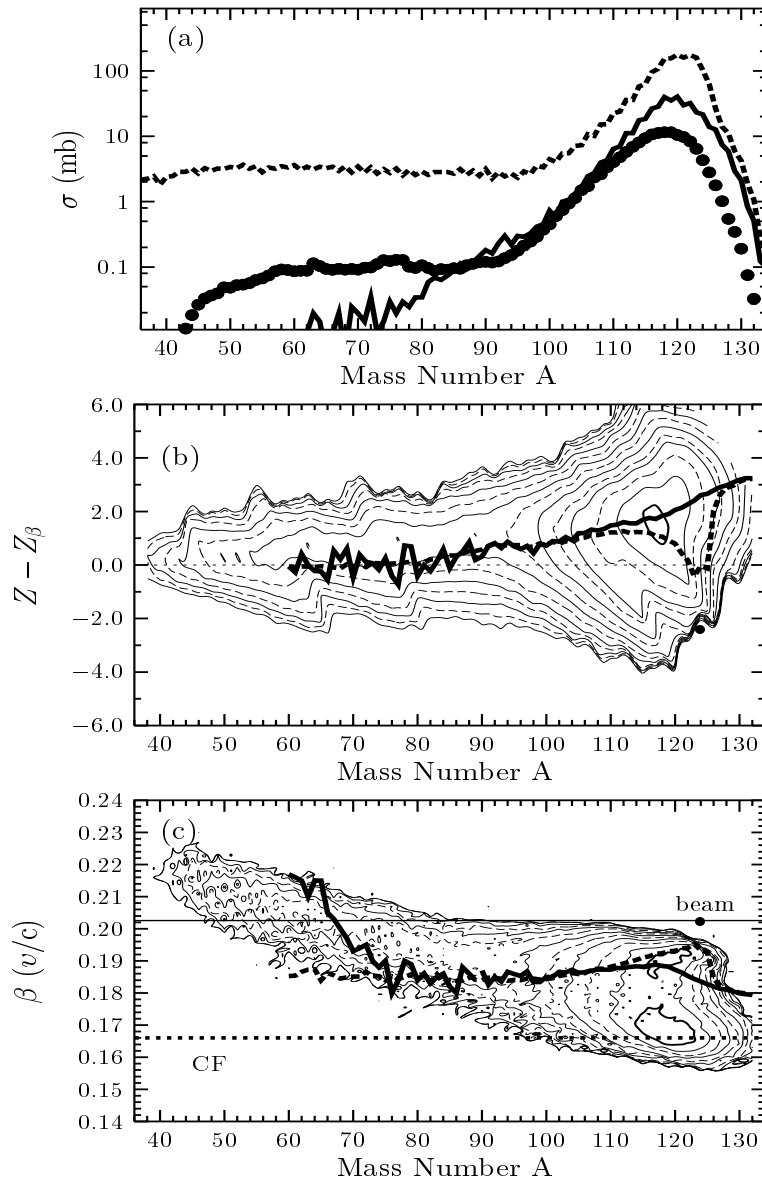


Fig. 3. Fragment distributions for the reaction $20 \text{ AM eV } ^{124}\text{Sn} + ^{27}\text{Al}$. (a) - isobaric yield distribution. The data are shown as solid circles. The dashed line is the result of DIT + ICF/GEM IN I (see text). The full line is the result of the same calculation as the dashed line, but with a cut corresponding to the angular and momentum acceptance of the spectrometer. (b) - yield distributions as a function of Z (relative to the line of stability, Z_β) and A . The calculated values from DIT + ICF/GEM IN I are shown as i) thick dashed line: without acceptance cut and, ii) thick full line: with acceptance cut. (c) - velocity vs. mass distributions. Data are shown as contours. The thick lines are as in (b). The horizontal full line represents the beam velocity and the horizontal dashed line represents the velocity of compound nucleus in the case of complete fusion.

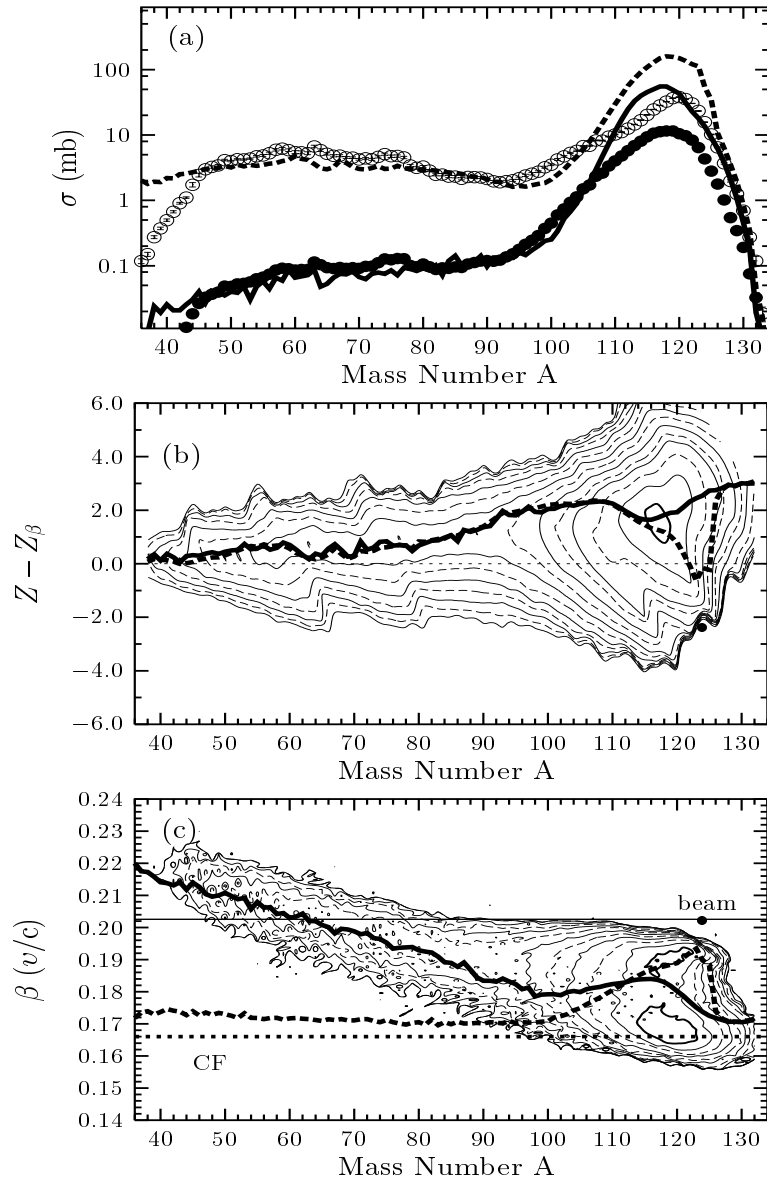


Fig. 4. Fragment distributions for the reaction 20 AM eV $^{124}\text{Sn} + ^{27}\text{Al}$ as in Fig. 3, except that the calculations are DIT + ICF/SM M. Open circles in (a) show estimated total cross sections (see text).

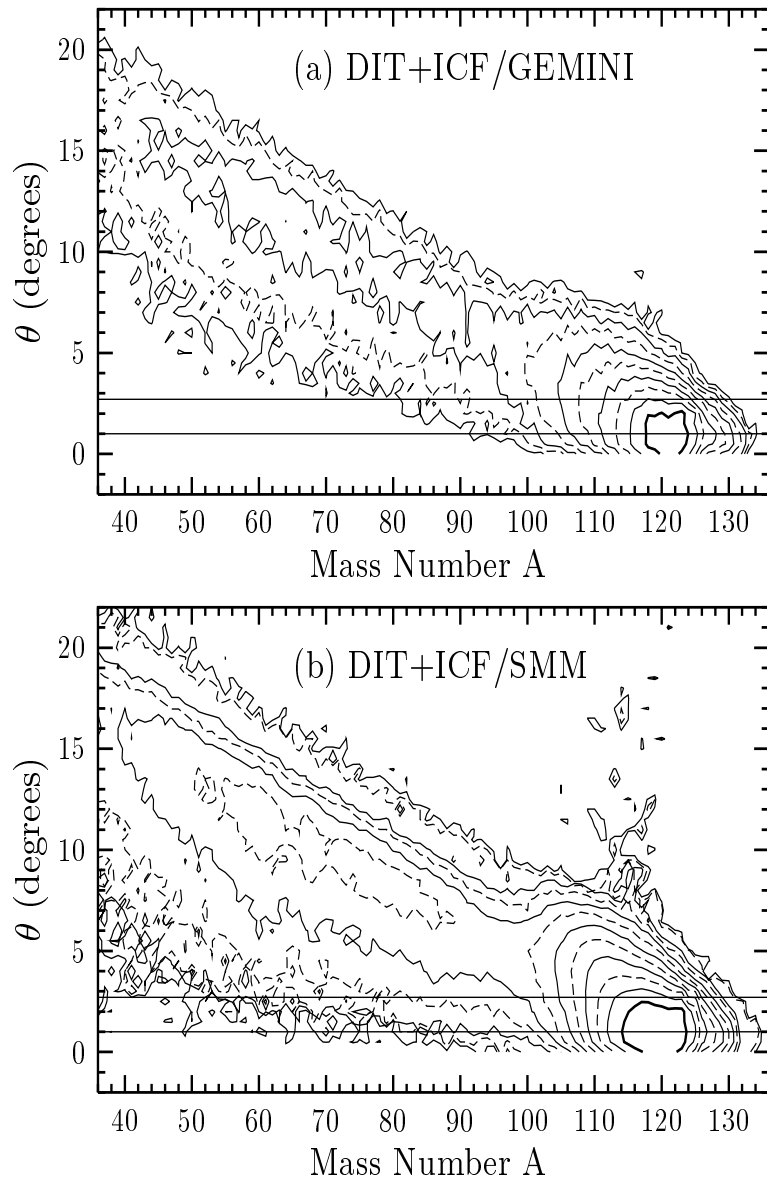


Fig. 5. Calculated angular distributions for the reaction $20 \text{ AM eV } ^{124}\text{Sn} + ^{27}\text{Al}$ as a function of residue mass for GEMINI (a) and SMM (b). The two horizontal lines mark the angular acceptance of the MARS separator.

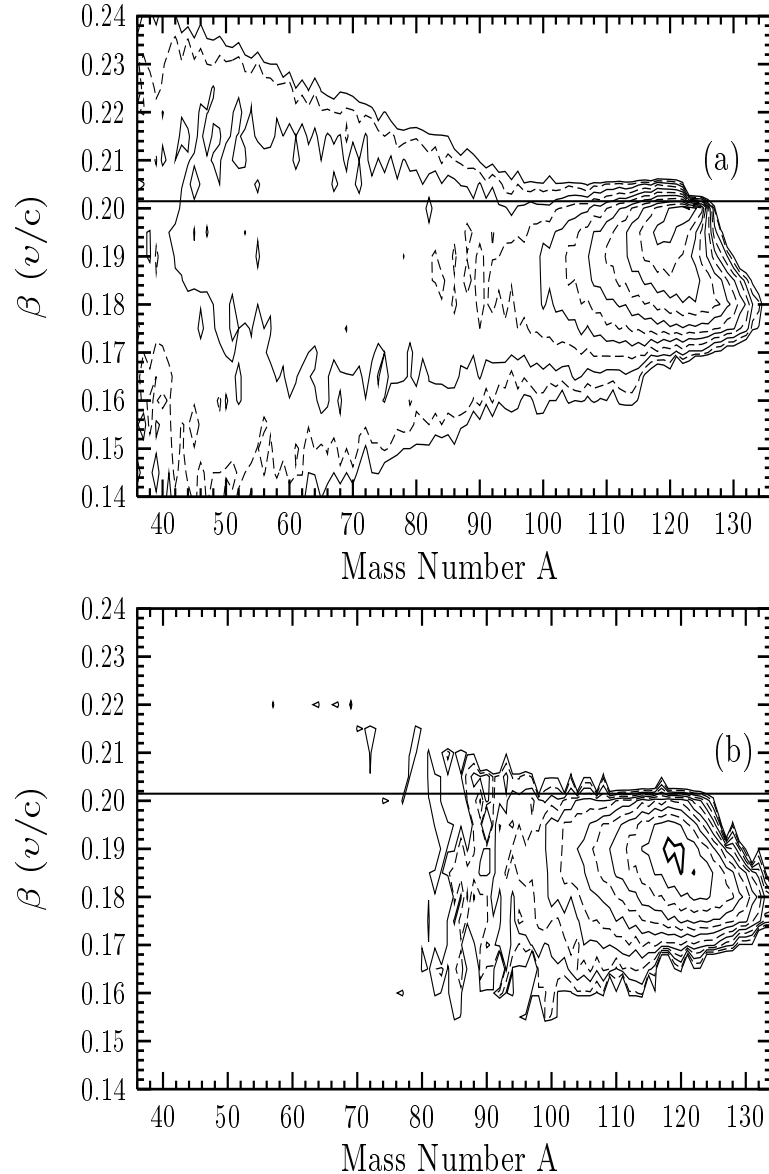


Fig. 6. Calculated velocity distributions for the reaction $20 \text{ AM eV } ^{124}\text{Sn} + ^{27}\text{Al}$ as a function of mass obtained using DIT + ICF / GEMINI simulation. Uniterated yields are presented in panel (a), while the iterated yields are given in panel (b). Horizontal lines mark the beam velocity.

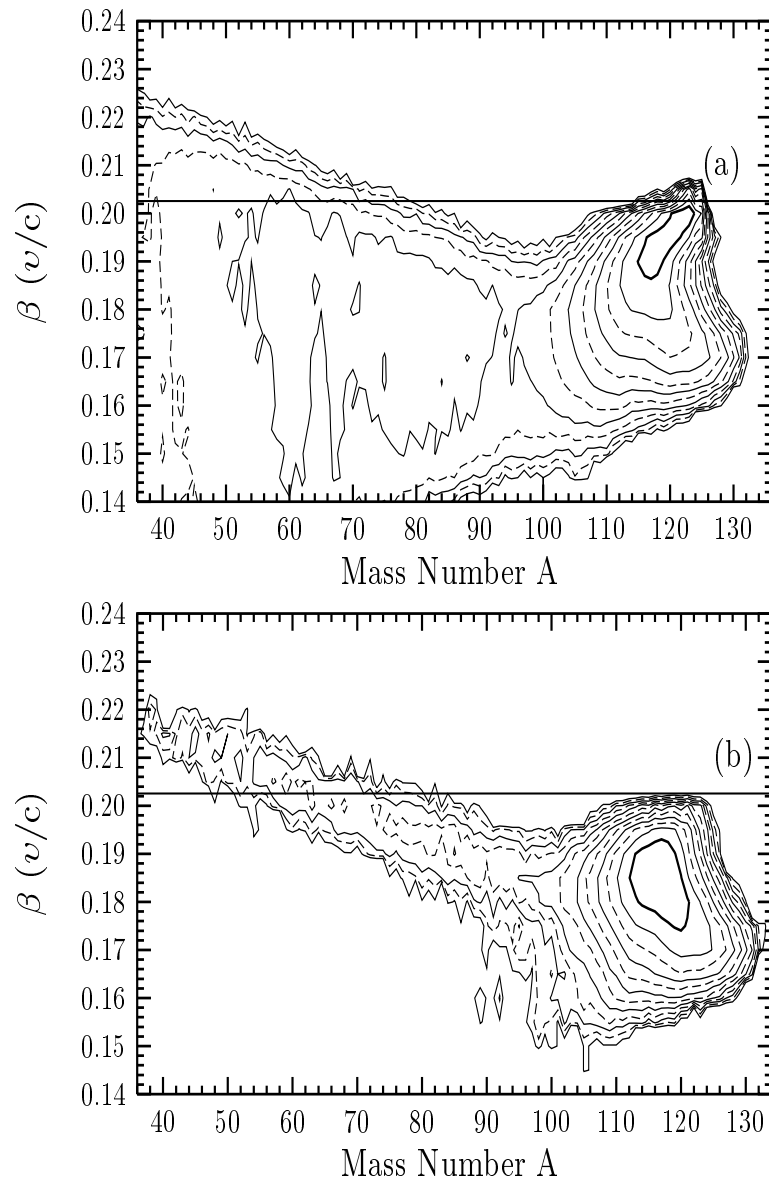


Fig. 7. Calculated velocity distributions for the reaction $20 \text{ AM eV } ^{124}\text{Sn} + ^{27}\text{Al}$ as a function of mass obtained using DIT + ICF/SM simulation. Unfiltered yields are presented in panel (a), while the filtered yields are given in panel (b). Horizontal lines mark the beam velocity.

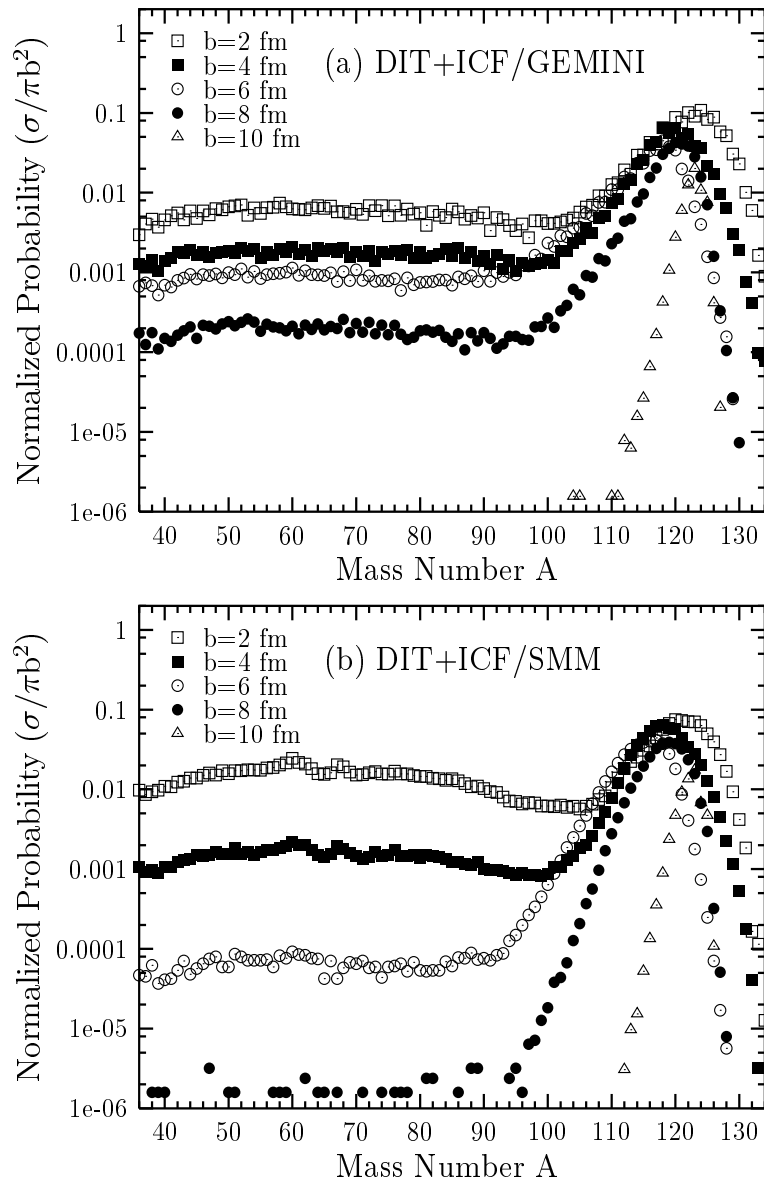


Fig. 8. Normalized unfiltered residue mass distributions for the reaction 20 AM eV $^{124}\text{Sn} + ^{27}\text{Al}$ at various impact parameters obtained using DIT+ICF/GEMINI (a), and DIT+ICF/SMM (b) simulations.

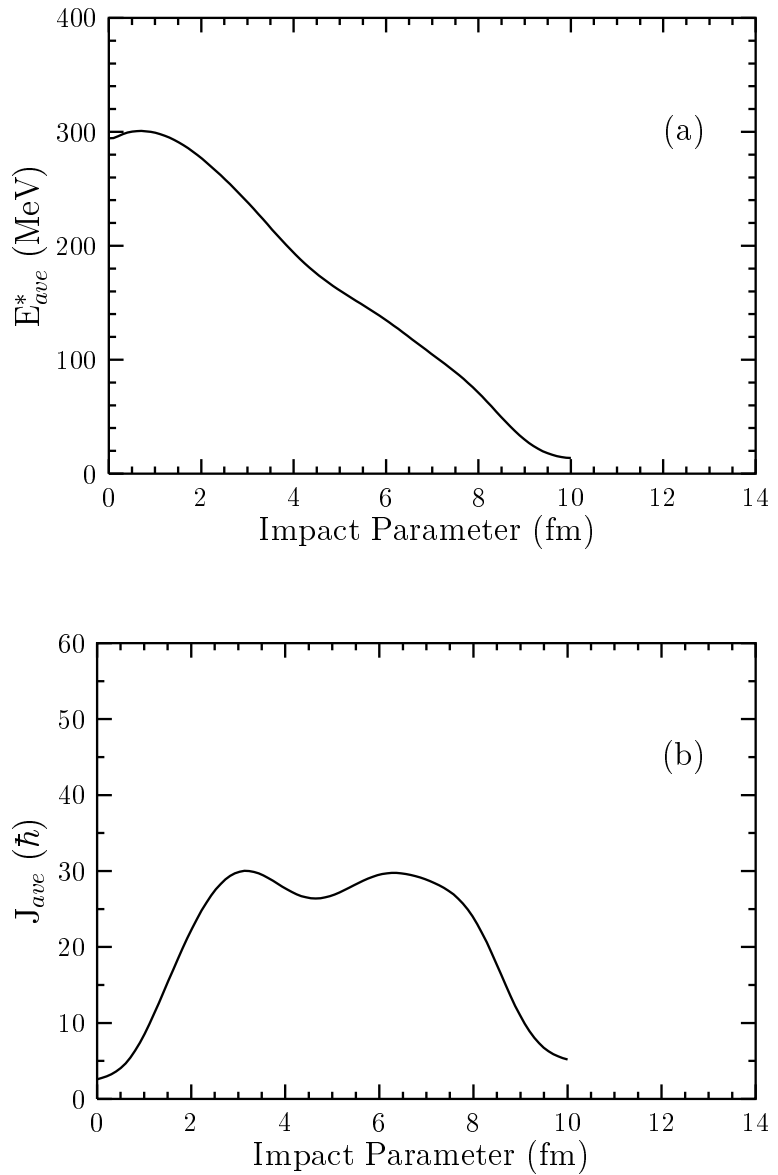


Fig. 9. Average excitation energy (a) and angular momentum (b) of the heavy source as a function of impact parameter obtained for the reaction 20 AM eV $^{124}\text{Sn} + ^{27}\text{Al}$ using DIT + ICF simulation.

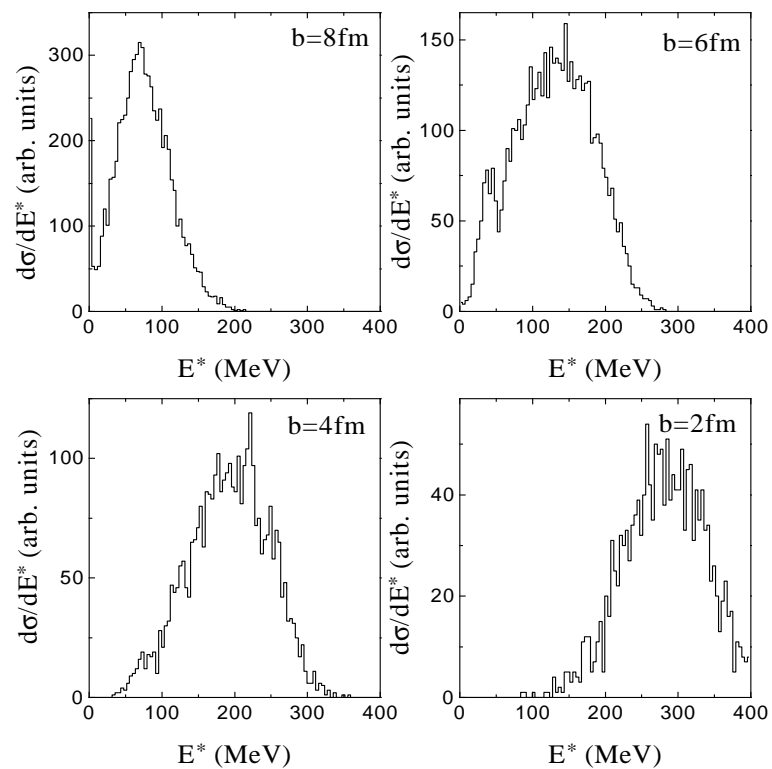


Fig. 10. Simulated excitation energy distribution of the heavy source at various impact parameters obtained for the reaction 20 AM eV $^{124}\text{Sn} + ^{27}\text{Al}$ using DIT + ICF simulation.